Energy 262 (2023) 125624

Contents lists available at ScienceDirect

Energy

journal homepage: www.elsevier.com/locate/energy

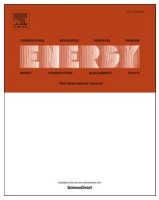

Optimal energy management of multiple electricity-hydrogen integrated charging stations

Xiaolun Fang [a], Yubin Wang [a], Wei Dong [a], Qiang Yang [a,*], Siyang Sun [b]

[a] College of Electrical Engineering, Zhejiang University, Hangzhou, 310027, China
[b] Energy Development Research Institute, China Southern Power Grid, China

ARTICLE INFO

Keywords:
Multiple EHI-CSs
PV systems
HES system
EMS strategy
MPC

ABSTRACT

Hydrogen is considered promising for the replacement of fossil fuels in integrated energy systems through hydrogen energy storage (HES). This paper considers multiple electricity-hydrogen integrated charging stations (EHI-CSs) as a unit consisting of photovoltaic systems and HES systems for charging plug-in electric vehicles and refilling hydrogen fuel vehicles. In the multiple EHI-CSs unit, a set of interconnected EHI-CSs can be supplied by other EHI-CSs or power utilities and an EHI-CSs aggregator can manage the individual EHI-CSs through controllable facilities (i.e., HES system) and adjustment methods (i.e., energy transportation between subsystems). Meanwhile, a two-stage energy management system (EMS) strategy is proposed to coordinate the day-ahead scheduling and real-time dispatch. In the day-ahead scheduling stage, the aggregator minimizes the cost of the overall multiple EHI-CSs unit through optimization, and in the real-time dispatching stage, the intraday energy dispatch based model predictive control (MPC) is carried out to minimize the penalty cost. The proposed two-stage EMS strategy is evaluated through simulations and the numerical results confirm that the proposed solution outperforms the baseline solution with additional economic benefit.

1. Introduction

Due to the exhaustion of fossil fuels and the pursuit of low-carbon energy provision across the world, the deployment of eco-friendly vehicles and renewable energy sources receives increasing attention [1]. Hydrogen fuel vehicles (HFVs) and plug-in electric vehicles are considered promising for their features of fast refueling rate, high mileage range and zero pollution to cope with the environmental concerns of internal combustion engine vehicles [2]. The widespread deployment of charging stations for HFVs, i.e. hydrogen fueling stations (HFSs), over the transportation infrastructure is fundamental to the hydrogen economy [3]. Meanwhile, photovoltaic (PV) power generation becomes one of the major renewable power sources in the modern power industry [4]. However, the intermittency of PV generation needs to be accommodated and managed through energy storage systems, e.g., Hydrogen Energy Storage (HES) systems, to ensure system stability [5]. HES system can produce hydrogen through power-to-hydrogen (P2H) based on water electrolyzers, store hydrogen in storage tanks and produce electricity using hydrogen-to-power (H2P) technology in fuel cells [6]. In recent years, due to the high energy density and long lifetime of hydrogen-based storage technologies, the exploitation of HES systems has attracted more and more attention [7]. For this regard, this work considers each electricity-hydrogen integrated charging station (EHI-CS) consisting of PV systems and HES systems for charging plug-in electric vehicles (PEVs) and refilling hydrogen fuel vehicles (HFVs).

The HFSs are expected for hydrogen production to meet the demand of HFVs [8], and recent studies have focused on the planning of HFSs. In Ref. [9], the authors designed an off-grid charging station consisting of a PV system, HES system and diesel system for electric and hydrogen vehicles. The optimal rated power for a PV system and diesel generator was determined to minimize the investment and operational costs. The location (i.e. sitting) problem of hydrogen fueling stations (HFSs) was studied in Refs. [10–12]. In Ref. [10], the multi-objective and multi-period HFSs location problem considered the combination of cost, risk and population coverage for the long-term planning. In Ref. [11], the authors presented a two-step pricing-based location strategy for new HFSs considering the depreciation cost, fixed cost and hydrogen selling price of the existing stations to maximize the profit of a new HFS. However, HFS in Refs. [10,11] only considered the onsite hydrogen production and storage with P2H technology without the consideration of the H2P process. In Ref. [12], the authors integrated H2P into the HFSs and placed the charging stations in the selected bus terminals for refilling hydrogen and electricity considering the subsidies and

* Corresponding author.
E-mail address: qyang@zju.edu.cn (Q. Yang).

https://doi.org/10.1016/j.energy.2022.125624
Received 29 April 2022; Received in revised form 25 August 2022; Accepted 28 September 2022
Available online 1 October 2022

Nomenclature

t Index of time steps
m Index of EHI-CSs
r Index of PEVs
Δt Time interval of the optimization problem (h)
T Optimization horizon (h)
t^{st} Starting time interval of the current MPC round
F_t^e The electricity cost of the unit ($)
F_t^{P2H} The cost by P2H mode ($)
F_t^{H2P} The cost by H2P mode ($)
$F_{gird,t}^{e,DM}$ Electrical power transaction cost in the day-ahead scheduling plan ($/kWh)
$C_{unit,t}^{im}$ Imbalance cost for RTM participation ($/kWh)
$C_{CS,m,t}^{e,RTM}$ Electrical power transaction cost between EHI-CSs ($/kWh)
$C_{unit,t}^{total}$ The actual total cost of the multiple EHI-CSs unit in the time period t ($)
$P_{unit,t}^{buy}$ Electrical power purchased from the utility grid to the unit (kW)
$P_{unit,t}^{sell}$ Electrical power sold from the unit to the utility grid (kW)
$P_{CS,m,t}^{buy}/P_{CS,m,t}^{sell}$ Electrical power purchased/sold from one EHI-CS to the other EHI-CS (kW)
$P_{all,m,t}^{buy}/P_{all,m,t}^{sell}$ Total electrical power purchased/sold for each power station (kW)
$P_{unit,t}^{gird}$ Electrical power exchanged with the utility grid for the day-ahead schedule (kW)
$P_{unit,t}^{gird,intra}$ Actual electrical power exchanged with the utility grid (kW)
$P_{unit,t}^{im}$ Imbalance power of the deviation between the day-ahead schedule and real-time dispatch (kW)
$Y_t^{buy,e}/Y_t^{sell,e}$ Price of buying/selling electricity of day-ahead clearing price ($/MWh)
$Y_t^{im,below}$ Negative imbalance price ($)
$Y_t^{im,excess}$ Positive imbalance price ($)
CC^{we}/CC^{fc} Capital cost for water electrolyzers and fuel cells ($)
$Hours^{we}/Hours^{fc}$ Number of life hours (h)
c^{we}/c^{fc} O&M cost function coefficient ($/h)
e^{we}/e^{fc} Start-up and shutdown cost function coefficients ($)
$\sigma_m^{P2H,on}/\sigma_m^{H2P,on}$ Start-up times of P2H/H2P mode
$\sigma_m^{P2H,off}/\sigma_m^{H2P,off}$ Shutdown times of P2H/H2P mode
$H_{m,t}^{HFV}$ HFVs load (kg)
$P_{m,t}^{PEV}$ PEV fast charging demand (kW)
$P_{m,t}^{Solar}$ Solar system power generation (kW)
$P_{used,m,t}^{Solar}$ PVs power generation utilized in actual (kW)
f_L Capacity of power line (kW)
E^{P2H} P2H conversion factor (kg/MWh)
E^{H2P} H2P conversion factor (MWh/kg)
η^{P2H}/η^{H2P} The efficiency of the P2H/H2P process (%)
$H_{m,t}^{we}$ Outflow hydrogen of water electrolyzer (kg/h)
$H_{m,t}^{fc}$ Inflow hydrogen of fuel cell (kg/h)
$P_{m,t}^{P2H}$ Input power of water electrolyzer (kW)
$P_{m,t}^{H2P}$ Output power of fuel cell (kW)
$I_{m,t}^{H2P}/I_{m,t}^{P2H}$ Binary status indicator of H2P/P2H
$P_{max}^{P2H}/P_{min}^{P2H}$ Maximum/Minimum input electric power of the HES systems (kW)
$P_{max}^{H2P}/P_{min}^{H2P}$ Maximum/Minimum output electric power of the HES systems (kW)
$HS_{m,t}$ Stored hydrogen in the hydrogen tank (kg)
HS_{max}/HS_{min} The maximum/minimum value of stored hydrogen (kg)
$HS_{m,ini}$ Initial stored hydrogen (kg)
r_t^{PEV} V2G subsidy from EHI-CSs
$C_{m,r,t}^{PEV}$ Capacity of the PEV for the rth PEV (kWh)
$P_{m,r,t}^{PEV,ch}/P_{m,r,t}^{PEV,disc}$ Charging and discharging power (kW)
$\eta^{PEV,ch}/\eta^{PEV,disc}$ Charging and discharging PEV efficiency (%)
$CR_{max}^{PEV}/DR_{max}^{PEV}$ Maximum PEV charging/discharging rate (kWh)
$I_{m,r,t}^{PEV,ch}/I_{m,r,t}^{PEV,disc}$ Binary status indicator of PEV charging/discharging
$SOC_{m,r,t}^{PEV}$ Stored energy in the PEV battery (%)
$SOC_{m,r}^{PEV,arr}$ SOC of the PEV battery when arriving (%)
$SOC_{m,r}^{PEV,dep}$ Required SOC of the PEV battery when departing (%)
$\Gamma_{m,r}^{arr}/\Gamma_{m,r}^{dep}$ Arrival/Departure time
$SOC_{min}^{PEV}/SOC_{max}^{PEV}$ Minimum/Maximum storage energy in the PEV battery (%)

governmental promotions for daily profit improvement of EHI-CSs. Here, the uncertainties due to weather, market price and EVs are considered, but the dynamics of hydrogen vehicles were not considered.

Some studies considered that HFSs are owned by different independent utilities and can participate in the electricity market. A model for the central scheduling of HFSs in the power distribution network was proposed in Ref. [13], and dynamic hydrogen pricing mechanisms were incorporated into the model to achieve the expected profit through adjusting hydrogen sale prices. In Ref. [14], a cooperative operation model for the WT and HFSs considering individual benefit was proposed based on the Nash bargaining theory, and the day-ahead cooperative operation was exploited to reduce the hydrogen production cost in HFSs. Likewise, the EHI system in Refs. [13,14] have not considered the process of H2P. In Ref. [15], HFSs were considered to provide operating reserve (OR) to an electricity market and it is confirmed that the HFS profit was improved when the stations participate in the OR market. In Ref. [16], an optimal day-ahead scheduling strategy for a microgrid with charging stations for PEVs and HFVs was proposed to meet the demand of hydrogen, heat and electricity considering the transaction of hydrogen and electricity with the grid.

In addition, much effort has been made to optimally schedule the microgrid without focusing on the penetration of HFSs for supplying HFVs' demand, i.e., the microgrid integrated with HES. In Ref. [17], considering the investment cost of the WT and HES system and the energy cost, a distribution network expansion planning for optimal siting and sizing of wind turbines (WT) and HES system was presented validated in the IEEE 33-bus network. Likewise, the work in Ref. [18] focused on the interaction between WT and HES system and developed a stochastic day-ahead scheduling model with the price-based demand response. In Ref. [19], a long-term optimal planning model was developed for the hybrid energy system containing electricity, heating, cooling and hydrogen demands with the considerations of P2H and hydrogen storage. In Ref. [20], the coordination and optimization operational model for an electric heat hydrogen multi-energy storage system was proposed to reduce the curtailment of WT and PV to the power grid and improve the flexibility of the power grid regulation.

To maintain dynamic energy supply and demand balances, energy management is essential to manage and coordinate the dispatchable

devices in the microgrids. In recent years, reinforcement learning (RL)-based algorithms have been considered a promising solution for solving the energy management problem without any *a priori* knowledge or effort of stochastic modeling. For example, the work in Ref. [21] proposed a cooperative RL-based algorithm for distributed economic dispatch in microgrids to coordinate the actions of distributed generation units and energy storage devices. In Ref. [22], an RL-based dynamic economic dispatch solution was proposed to minimize the total generation cost with no knowledge of the mathematical formulation of the actual generation cost functions. However, these solutions often require a long learning time and sophisticated learning policies. These increase the computational complexity of the real-time implementation of the RL-based solution [23]. The model predictive control (MPC)-based method can also be applied in the intraday dispatch based on the prediction information and rolling optimization. In Ref. [24], an MPC-based model is established to schedule the operation based on the short-term prediction information, and its dispatch result is adjusted based on ultra-short-term error prediction. In Ref. [25], a supervisory energy management strategy for a standalone microgrid is designed based on the MPC method incorporated with forecasting techniques.

For the coordination and optimization operation of electricity and hydrogen, some work considered the day-ahead market (e.g. Refs. [14, 16,18]), whereas little work has considered the flexible coordination of day-ahead scheduling and real-time dispatch in the integration of electricity and hydrogen. In Ref. [26], an energy management model considering the optimal coordination of HFSs with demand response (DR), energy storage systems (ESS) as well as the day-ahead and real-time markets mechanisms was proposed. However, the H2P process was not considered to respond to the electricity pricing changes. In Ref. [27], a MPC-based method was developed for optimal economic scheduling of MG based on three types of energy storage systems (i.e., ESS, ultra-capacitor and HES) considering time-varying prices. In Ref. [28], a two-stage model based on robust optimization was proposed to minimize the operation cost of an HFS through the management of electricity price uncertainties.

It can be observed that existing studies exploited the participation of microgrid integrated electric and hydrogen energy in the electricity market without the consideration of the coordination among multiple charging stations integrated with HES systems. To this end, this works exploits an optimal energy management strategy among multiple physically decentralized EHI-CSs that are managed by an EHI-CSs aggregator for fast-charging PEVs and refilling HFVs. A set of interconnected EHI-CSs can realize the power coordination among multiple EHI-CSs, and the HES system is utilized to accommodate the uncertainties of generation and load. Also, the optimal energy management of EHI-CSs can promote profit through participation in the deregulated power market. The main technical contributions made in this work can be summarized as follows.

(1) A multiple EHI-CSs unit containing a set of interconnected EHI-CSs for fast-charging PEVs and refilling HFVs is established in this work. Electricity transactions among EHI-CSs and controllable facilities (i.e., water electrolyzers and fuel cells) can realize flexible energy management to participate in the electricity market.
(2) A two-stage energy management system (EMS) strategy of multiple EHI-CSs unit is proposed to minimize the daily cost of the unit through the coordination of day-ahead scheduling in the day-ahead market (DM) and MPC-based real-time dispatch in the real-time market (RTM).
(3) The proposed energy management solution is extensively assessed through a case study of multiple EHI-CSs unit with three EHI-CSs compared against two benchmark solutions (i.e., no transaction among EHI-CSs and no intra-day corrections), and the numerical results confirm its economic benefits.

The remainder of this paper is organized as follows: Section 2 presents the multiple EHI-CSs unit model and the proposed EMS strategy. Section 3 describes the day-ahead scheduling and real-time dispatch model. The proposed EMS strategy is assessed in Section 4. Finally, the conclusive remarks are given in Section 5.

2. System model and proposed solution

This section presents the model of the multiple EHI-CSs unit and the electricity market for developing the proposed EMS.

2.1. Overview of the proposed system

The structure of a multiple EHI-CSs unit is illustrated in Fig. 1, and the communication connections between EHI-CSs and grid through a point of common coupling (PCC) and the EHI-CSs aggregator are also illustrated in the figure. For the electrical power transmission, EHI-CSs can supply and absorb electricity by both utility and other EHI-CSs. In the multiple EHI-CSs unit, EHI-CSs are considered physically adjacent and connected with the grid through the same power line. Several EHI-CSs are connected to the gird through a PCC and the line limitation in PCC is equal to f_L [29].

The local power generation sources and load data within each EHI-CS are collected by a local controller (LC) and made available to the EHI-CSs aggregator for energy management. The role of the EHI-CSs aggregator is to minimize the economic cost of the whole multiple EHI-CSs unit [30]. It is noteworthy to mention that, in the proposed multiple EHI-CSs unit structure, the number of charging stations can be increased based on power system planning.

The EHI-CS for PEVs and HFVs consists of a PV system, a HES system (including an electrolyzer, hydrogen tanks and a fuel cell) and a set of electric and hydrogen loads (i.e., PEVs and HFVs), as illustrated in Fig. 2. In this work, an EHI-CS is a small-scale energy zone consisting of different forms of generation sources, including the undispatchable energy sources (e.g., PV systems) and the dispatchable energy sources (e.g., water electrolyzer and fuel cell). These power generation sources are used to supply the electric load (i.e. PEVs) and hydrogen load (i.e. HFVs) within each EHI-CS and the demands of other EHI-CSs when necessary. Also, the individual EHI-CSs are interconnected with the power utility to ensure power supply reliability and flexibility.

2.2. Electrical market model

The EHI-CSs aggregator that manages the multiple EHI-CSs unit participates in a deregulated energy market including DM and RTM. The DM is used to schedule the energy transaction for the next day and the RTM aims to balance the power supply and demand in real-time. In the DM, the EHI-CSs aggregator can estimate the one-day multiple EHI-CSs unit consumption profiles and makes it available to the market organizer

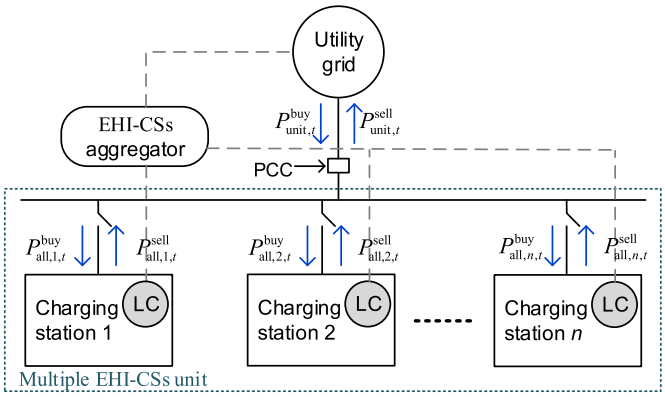

Fig. 1. System model for multiple charging stations and utility grid.

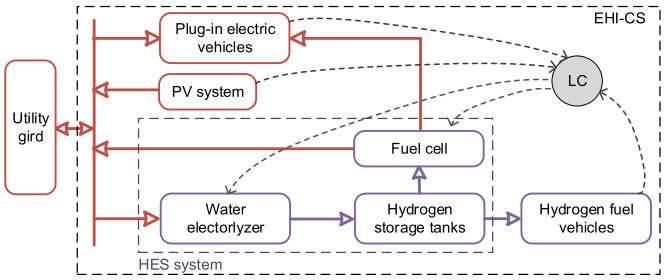

Fig. 2. Charging station for electric and hydrogen vehicles.

that will produce the day-ahead clearing price based on the power demand and supply profiles, as suggested in Ref. [31]. Due to the inevitable forecasting error of the day-ahead stage, in the RTM, the EHI-CSs aggregator needs to update the operational decisions to follow the day-ahead schedule [32]. Besides, RTM is based on a dual-pricing market where deviations from the agreed power exchange are penalized. In transactions with the grid, electricity power consumed below the scheduled is fined at a price lower than the day-ahead market price, whereas excess electricity power consumed is penalized at a price higher than the day-ahead market price [33].

2.3. Energy management strategy

The proposed two-stage EMS strategy is schematically illustrated in Fig. 3. More specifically, the EMS strategy developed in this paper can be divided into two stages, i.e. the day-ahead scheduling stage and the real-time dispatch stage.

In the day-ahead scheduling stage, based on the day-ahead clearing price, the day-ahead predicted data for RESs power generation and the demand, the minimum daily cost of the EHI-CSs unit can be obtained. The hourly optimal output curve of each generation source and the hourly optimal electric power exchange with the grid can be also obtained, as well as the electric exchange between the EHI-CSs. Then, the scheduling plan will be sent to the real-time dispatch stage.

In the real-time dispatch stage, the real-time dispatch revises the day-ahead schedule based on the RTM and short-term forecasted data to minimize the daily cost of the EHI-CSs unit using an MPC-based real-time optimization approach. MPC is an iterative and finite-time optimization method that provides an effective solution to reduce the impact of prediction errors [34]. In the optimization, only the computed control signal of the current time interval is applied to the real-time dispatch process. In the next time step, the receding window is shortened by a one-time slot, and the intra-day energy dispatch algorithm repeats [32]. Note that, the short-term predicted data is used for the first several time slots of the optimization horizon, and the day-ahead forecasted data are used for the remaining intervals to ensure that each step of optimization takes into account constraints and information of the whole day. The MPC-based real-time optimization process in the proposed two-stage EMS is illustrated in Fig. 3.

3. Problem formulation

The day-ahead scheduling model with the DM participation and the real-time dispatch model with the RTM participation are described in this section, as well as the constraints for PV power generation, HES systems and power balance.

3.1. Day-ahead scheduling model

According to the day-ahead clearing price and the forecasted data of PV power generation, PEV and HFV load, the EHI-CSs aggregator makes its economic optimization schedule to minimize the daily cost of the multiple EHI-CSs unit. The objective function of the day-ahead sched-

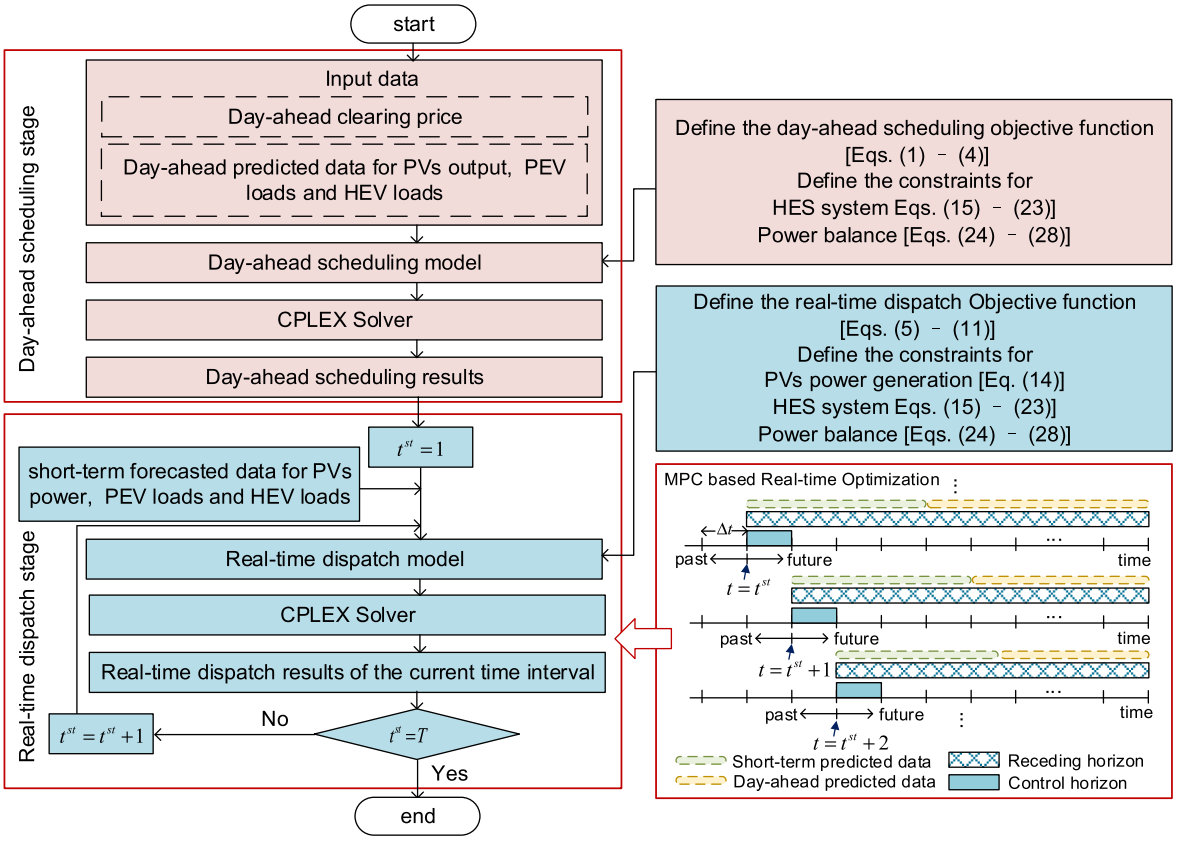

Fig. 3. The schematic diagram of the proposed two-stage EMS solution.

uling model is as Eqs. (1)–(4).

$$\min OF = \sum_{t=1}^{T}\left(F_t^{\mathrm{e}} + F_t^{\mathrm{P2H}} + F_t^{\mathrm{H2P}}\right)\Delta t \tag{1}$$

$$F_t^{\mathrm{e}} = \sum_{m=1}^{M} Y_t^{\mathrm{buy,e}} P_{\mathrm{all},m,t}^{\mathrm{buy}} - Y_t^{\mathrm{sell,e}} P_{\mathrm{all},m,t}^{\mathrm{sell}} \tag{2}$$

$$F_t^{\mathrm{P2H}} = \sum_{m=1}^{M}\left(\left(\frac{CC^{\mathrm{we}}}{Hours^{\mathrm{we}}} + c^{\mathrm{we}}\right) I_{m,t}^{\mathrm{P2H}} + e^{\mathrm{we}}\left(\sigma_m^{\mathrm{we,on}} + \sigma_m^{\mathrm{we,off}}\right)\right) \tag{3}$$

$$F_t^{\mathrm{H2P}} = \sum_{m=1}^{M}\left(\left(\frac{CC^{\mathrm{fc}}}{Hours^{\mathrm{fc}}} + c^{\mathrm{fc}}\right) I_{m,t}^{\mathrm{H2P}} + e^{\mathrm{fc}}\left(\sigma_m^{\mathrm{fc,on}} + \sigma_m^{\mathrm{fc,off}}\right)\right) \tag{4}$$

The objective function is given in Eq. (1) that minimizes the total cost due to electricity transactions and the operating cost of the HES system. Eq. (2) denotes the cost of electric power transactions, including the electrical transaction with the utility grid and among EHI-CSs, in the time period t. Eqs. (3) and (4) are cost functions of the HES system in P2H and H2P modes, respectively. In these two equations, the first term represents the operation and maintenance (O&M) cost for the water electrolyzer and fuel cell, which is associated with the working hours; the second term denotes the degradation cost, which is mainly associated with their start-up and shut-down times [27,35]. The day-ahead scheduling model for DM participation needs to follow the constraints Eqs. (14)–(28), and the detailed constraints are explained in part *3.3*.

3.2. Real-time dispatch model

The inevitable difference between forecast data and real-time data may issue discrepancies between day-ahead schedule and real-time energy usage, resulting in a significant additional penalty for the power imbalance. The multiple EHI-CSs unit includes a large number of controllable facilities and adjustment methods for flexible coordination of day-ahead planning and real-time dispatching. In the RTM participation, the EHI-CSs aggregator should decrease the penalty cost as soon as possible to achieve its profit maximization. Notice, in the real-time dispatching, the electricity transactions between each EHI-CS and the operation of HES systems may differ from the day-ahead planning. Hence, the objective function of the multiple EHI-CSs unit for RTM participation should contain the penalty cost of energy imbalance, as well as the transaction cost between each EHI-CS and the operation cost of HES systems, which is shown in Eq. (5).

$$\min OF^{\mathrm{RTM}} = \sum_{t=t^{\mathrm{st}}}^{T}\left(F_t^{\mathrm{e,RTM}} + F_t^{\mathrm{P2H,RTM}} + F_t^{\mathrm{H2P,RTM}}\right)\Delta t \tag{5}$$

where the extra superscript "RTM" denotes the cost in the RTM participation. Different from the day-ahead scheduling model, as shown in Eq. (6), electricity power transaction cost in the RTM participation includes penalty cost of energy imbalance and the electrical transaction cost among EHI-CSs. The expected energy imbalance to be compensated in the RTM is modeled as (7) to (10). Eq. (11) represents the cost for each EHI-CS due to the electrical transactions among EHI-CSs in the time period t. Notice, in the real-time dispatch stage, the exchange of electricity between the EHI-CSs in the multiple EHI-CSs unit will continue at a previously agreed price (i.e., day-ahead clearing price). It should be noted here that the variables used in the intraday dispatch model are denoted with superscript "intra".

$$F_t^{\mathrm{e,RTM}} = C_{\mathrm{unit},t}^{\mathrm{im}} + \sum_{m=1}^{M} C_{\mathrm{CS},m,t}^{\mathrm{e,RTM}} \tag{6}$$

$$C_{\mathrm{unit},t}^{\mathrm{im}} = \begin{cases} Y_t^{\mathrm{im,below}} \times P_t^{\mathrm{im}}, P_t^{\mathrm{im}} \le 0 \\ Y_t^{\mathrm{im,excess}} \times P_t^{\mathrm{im}}, P_t^{\mathrm{im}} \ge 0 \end{cases} \tag{7}$$

$$P_{\mathrm{unit},t}^{\mathrm{im}} = P_{\mathrm{unit},t}^{\mathrm{gird,intra}} - P_{\mathrm{unit},t}^{\mathrm{gird}} \tag{8}$$

$$P_{\mathrm{unit},t}^{\mathrm{gird}} = P_{\mathrm{unit},t}^{\mathrm{buy}} - P_{\mathrm{unit},t}^{\mathrm{sell}} \tag{9}$$

$$P_{\mathrm{unit},t}^{\mathrm{gird,intra}} = P_{\mathrm{unit},t}^{\mathrm{buy,intra}} - P_{\mathrm{unit},t}^{\mathrm{sell,intra}} \tag{10}$$

$$C_{\mathrm{CS},m,t}^{\mathrm{e,RTM}} = Y_t^{\mathrm{buy,e}} P_{\mathrm{CS},m,t}^{\mathrm{buy,intra}} - Y_t^{\mathrm{sell,e}} P_{\mathrm{CS},m,t}^{\mathrm{sell,intra}} \tag{11}$$

The expressions of $F_t^{\mathrm{P2H,RTM}}$ and $F_t^{\mathrm{H2P,RTM}}$ are similar to Eq. (3) and Eq. (4) in the day-ahead scheduling model, and the real-time dispatch model for RTM participation also needs to meet the constraints in Eqs. (14)–(28). For the sake of limited space, these equations are not repeated here. Further, from the day-ahead scheduling model and real-time dispatch model, it can be observed that, in the current time interval, the actual total cost of the multiple EHI-CSs unit can be described as,

$$C_{\mathrm{unit},t}^{\mathrm{total}} = F_{\mathrm{gird},t}^{\mathrm{e,DM}} + F_t^{\mathrm{e,RTM}} + F_t^{\mathrm{P2H,RTM}} + F_t^{\mathrm{H2P,RTM}} \tag{12}$$

$$F_{\mathrm{gird},t}^{\mathrm{e,DM}} = Y_t^{\mathrm{buy,e}} P_{\mathrm{unit},t}^{\mathrm{buy}} - Y_t^{\mathrm{sell,e}} P_{\mathrm{unit},t}^{\mathrm{sell}} \tag{13}$$

3.3. Constraints

In the multiple EHI-CSs unit, the balance of electric power and hydrogen power should be guaranteed.

1) Constraints of the PV generation system

Due to the penalty cost of energy imbalance, the light abandonment in PV systems may occur in MGs, and thus PVs power generation utilization is subject to Eq. (14).

$$0 \le P_{\mathrm{used},m,t}^{\mathrm{Solar}} \le P_{m,t}^{\mathrm{Solar}} \tag{14}$$

2) Constraints of HES system

The HES system consists of a water electrolyzer, hydrogen tank and fuel cell. In this system, when the HES is charged, the generated hydrogen by the water electrolyzer is stored in the hydrogen tank, and the produced hydrogen by the water electrolyzer is modeled by Eq. (15). On the other hand, when the HES is discharged, the fuel cell produces electricity from stored hydrogen, the consumed hydrogen to generate the electrical power by the fuel cell is calculated using Eq. (16).

$$H_{m,t}^{\mathrm{we}} = P_{m,t}^{\mathrm{P2H}} E^{\mathrm{P2H}} \eta^{\mathrm{P2H}} \tag{15}$$

$$P_{m,t}^{\mathrm{H2P}} = H_{m,t}^{\mathrm{fc}} E^{\mathrm{H2P}} \eta^{\mathrm{H2P}} \tag{16}$$

Eq. (17) guarantees that the H2P and P2H will not occur at the same time in the HES system. Eqs. (18) and (19) denote the upper and lower limits of hydrogen and power generated by the HES system.

$$I_{m,t}^{\mathrm{H2P}} + I_{m,t}^{\mathrm{P2H}} \le 1 \tag{17}$$

$$P_{\min}^{\mathrm{P2H}} I_{m,t}^{\mathrm{P2H}} \le P_{m,t}^{\mathrm{P2H}} \le P_{\max}^{\mathrm{P2H}} I_{m,t}^{\mathrm{P2H}} \tag{18}$$

$$P_{\min}^{\mathrm{H2P}} I_{m,t}^{\mathrm{H2P}} \le P_{m,t}^{\mathrm{H2P}} \le P_{\max}^{\mathrm{H2P}} I_{m,t}^{\mathrm{H2P}} \tag{19}$$

The hourly stored hydrogen for HES systems is given by(20) that is limited to the maximum and minimum tanks capacity, as shown in Eq. (21). In the initial period of the day, the initial amount of hydrogen in hydrogen storage tanks is given in Eq. (22), and Eq. (23) specifies that the initial value of the stored hydrogen at $t = 0$ is the same as the value at $t = T$.

$$HS_{m,t} = HS_{m,t-1} + H_{m,t}^{\mathrm{we}} - H_{m,t}^{\mathrm{fc}} - H_{m,t}^{\mathrm{HFV}} \tag{20}$$

$$HS_{\min} \le HS_{m,t} \le HS_{\max} \tag{21}$$

$$HS_{m,0} = HS_{m,\mathrm{ini}} \tag{22}$$

$$HS_{m,T} = HS_{m,0} \tag{23}$$

3) Power balance constraints

The electrical power balance constraints of the multiple EHI-CSs unit and the mth EHI-CS in each time slot is defined as (24) and (25), respectively.

$$P^{\mathrm{buy}}_{\mathrm{unit},t} - P^{\mathrm{sell}}_{\mathrm{unit},t} = \sum_{m=1}^{M}\left(P^{\mathrm{buy}}_{\mathrm{all},m,t} - P^{\mathrm{buy}}_{\mathrm{CS},m,t}\right) - \sum_{m=1}^{M}\left(P^{\mathrm{sell}}_{\mathrm{all},m,t} - P^{\mathrm{sell}}_{\mathrm{CS},m,t}\right) \tag{24}$$

$$P^{\mathrm{Solar}}_{\mathrm{used},m,t} + P^{\mathrm{H2P}}_{m,t} - P^{\mathrm{P2H}}_{m,t} - P^{\mathrm{PEV}}_{m,t} = P^{\mathrm{sell}}_{\mathrm{all},m,t} - P^{\mathrm{buy}}_{\mathrm{all},m,t} \tag{25}$$

Eq. (26) guarantees the multiple EHI-CSs unit either receiving power or sending power to the utility grid. Eqs. (27) and (28) are used to ensure that the transmission power between the multiple charging stations unit and the utility grid cannot exceed the line limitation in the PCC.

$$I^{\mathrm{buy}}_{\mathrm{unit},t} + I^{\mathrm{sell}}_{\mathrm{unit},t} \le 1 \tag{26}$$

$$0 \le P^{\mathrm{buy}}_{\mathrm{unit},t} \le f_{\mathrm{L}} \times I^{\mathrm{buy}}_{\mathrm{unit},t} \tag{27}$$

$$0 \le P^{\mathrm{sell}}_{\mathrm{unit},t} \le f_{\mathrm{L}} \times I^{\mathrm{sell}}_{\mathrm{unit},t} \tag{28}$$

4. Simulation experiments and numerical results

To evaluate the effectiveness of the proposed MPC-based EMS strategy, a multiple EHI-CSs unit consisting of three EHI-CSs is considered with the DM and RTM participation. The problem is implemented in the YALMIP modeling language as linear programming and solved using the CPLEX optimizer [36]. In this work, the i7-97000 CPU, @3.20 GHz and 16.00 G RAM are used for computation hardware, and the optimization is performed in MATLAB (version 2018a). The executive time for decision-making of the day-ahead energy scheduling is 3.28 s. The execution time of the real-time energy dispatch for a one-time slot decreases from 2.3 s to 0.47 s along with the window receding. This indicates that the proposed energy management solution can be carried out in an online fashion for the multiple EHI-CSs unit.

4.1. Simulation setup

The time slot in the implemented model is set as 1 h, i.e., in total 24-time slots over a day. For three EHI-CSs, the maximum power capacities of PVs generation are set as 1.2 MW, 2.6 MW and 1.4 MW; the maximum charging capacities for PEVs are set as 0.9 MW, 0.6 MW and 0.6 MW; the maximum charging capacities for HEVs are set as 70 kg, 40 kg, and 30 kg, respectively. The capacity of power line is set as 1.5 MW, and to leave some space for intraday dispatching, the capacity of power line in the day-ahead scheduling stage is set as 1.35 MW. The corresponding parameters of the HES system are given in Table 1, as suggested in Refs. [35,37]. The hourly day-ahead clearing electricity price, the predicted and real data for the PV systems generation, PEV loads and HFV loads used in this test are shown in Fig. 4(a)–(d), respectively, as extracted from Refs. [15,37–41]. The predicted data is obtained by adding a forecast error to the real data [42]. The forecast errors of PVs are assumed to follow beta distributions [43]. It is assumed that the power forecast errors in the microgrid follow the same distribution due to the similar environment [7], and the predictions are with the normalized root mean squared error of 10%, as suggested in Ref. [44]. Further, it is considered that the day-ahead selling price is 0.9 times the day-ahead purchasing price, i.e. $Y^{\mathrm{sell,e}}_t = 0.9Y^{\mathrm{buy,e}}_t$ [45], and for the real-time energy market, the positive/negative imbalance price is 2/0.8 times the day-ahead purchasing price, i.e. $Y^{\mathrm{im,excess}}_t = 2Y^{\mathrm{buy,e}}_t$ and $Y^{\mathrm{im,below}}_t = 0.8Y^{\mathrm{buy,e}}_t$ [46], respectively.

Unlike the day-ahead prediction, the intra-day forecast is carried out on a short-term scale (4 h), and thus can be considered close to the actual value [32]. In this work, for the receding horizon, the real data has been adopted for the first four-time slots and the day-ahead predicted data is used for the remaining time slots.

Table 1
The required parameters for modeling the HES system.

Parameter	Value	Parameter	Value
$P^{\mathrm{P2H}}_{\max}/P^{\mathrm{P2H}}_{\min}$ (MW)	1/0.1	$\eta^{\mathrm{P2H}}/\eta^{\mathrm{H2P}}$ (%)	0.8/0.6
$P^{\mathrm{H2P}}_{\max}/P^{\mathrm{H2P}}_{\min}$ (MW)	1/0.1	$CC^{\mathrm{we}}/CC^{\mathrm{fc}}$ ($)	$1.25 \times 10^5/1.0 \times 10^5$
$HS_{\max}/HS_{\min}$ (kg)	300/30	$Hours^{\mathrm{we}}/Hours^{\mathrm{fc}}$(h)	50,000/20,000
$HS_{m,\mathrm{ini}}$ (kg)	80	$c^{\mathrm{we}}/c^{\mathrm{fc}}$ ($/h)	0.07/0.05
E^{P2H} (kg/kWh)	0.0254	$e^{\mathrm{we}}/e^{\mathrm{fc}}$ ($)	0.38/0.05
E^{H2P} (kWh/kg)	39.4		

4.2. Day-ahead scheduling results

Day-ahead scheduling results for exchanging electric power with the gird over the test day are illustrated in Fig. 5, where the positive/negative values indicate the purchased/sold power.

Fig. 6 presents the result of day-ahead electrical scheduling over the test day for three EHI-CSs. The input and output electric power of HES systems for three EHI-CSs in the day-ahead scheduling stage as well as the power exchange (with the power utilities or other EHI-CSs) are illustrated in Fig. 6. In these figures, the positive values of the bar chart indicate the power flowing into the EHI-CS, i.e. the PV power output, the required electric power by the electrolyzer to produce hydrogen and the

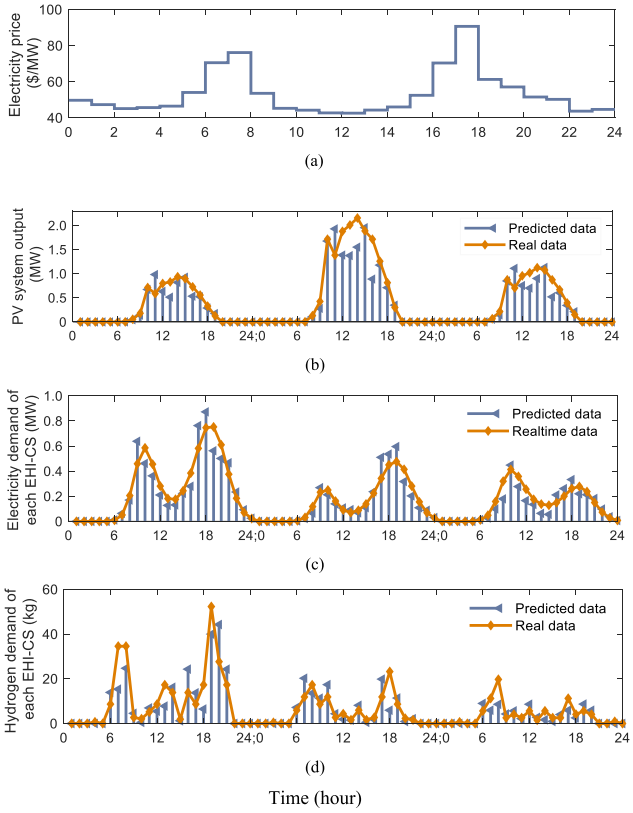

Fig. 4. Profiles of (a) day-ahead electricity price; (b) PV system output; (c) electricity demand for three EHI-CSs; and (d) hydrogen demand for three EHI-CSs.

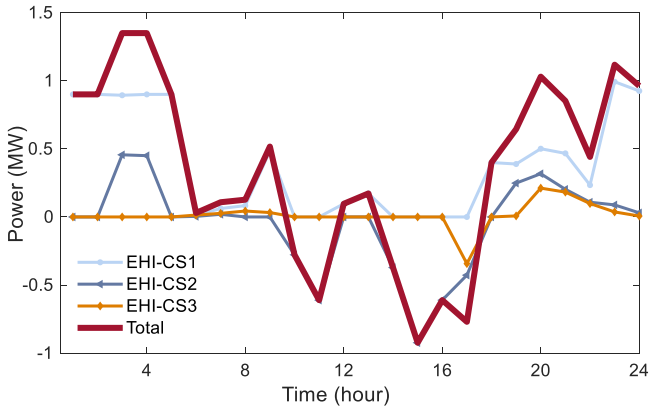

Fig. 5. The electric power exchange with the gird in the DM scheduling stage.

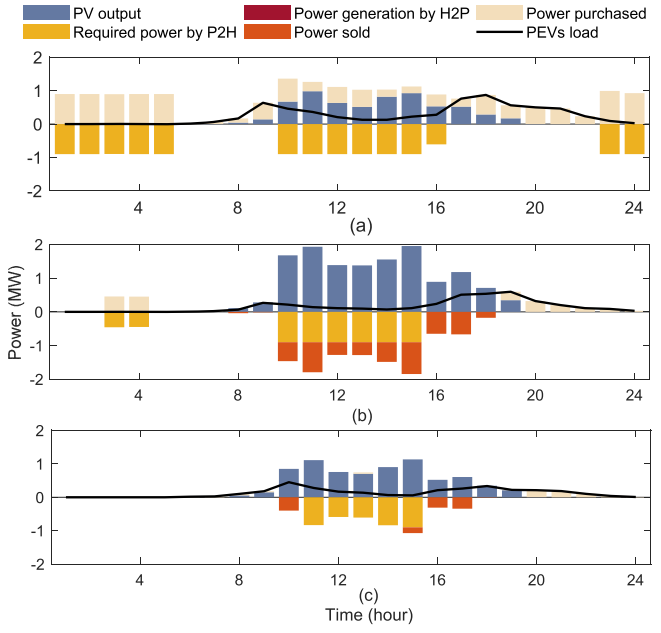

Fig. 6. The day-ahead electrical scheduling for (a) EHI-CS1; (b) EHI-CS2; and (c) EHI-CS3.

total purchased electrical power by each EHI-CS. The positive values represent the power supply by the fuel cell and the sold electricity. Fig. 7 presents the day-ahead hydrogen scheduling results over the simulated day for three EHI-CSs, i.e. the expected demand of HFVs (gray bars), the required hydrogen by the H2P process (red bars) and the produced hydrogen (yellow bars) that is used to supply the HFVs or stored in the tanks. Fig. 8 presents the day-ahead stored hydrogen in the tanks for three EHI-CSs. As can be seen from the figures, most of the hydrogen consumption behaviors happen in the daytime. The hydrogen production behaviors mostly happen during periods when the electricity price is low or the PV power is abundant. As the stored hydrogen should be kept to their initial level at the end of the day, the amount of stored hydrogen in three EHI-CSs returns to the same level at time 24. Further, it can be found that there is no H2P process in the day-ahead scheduling stage, which may be due to the low efficiency of H2P technology. The economic benefit of using H2P technology to obtain electricity is lower than purchasing electricity from outside. However, H2P technology can be used in the intraday dispatching stage to deal with the uncertainties to reduce the penalty cost of the RTM participation.

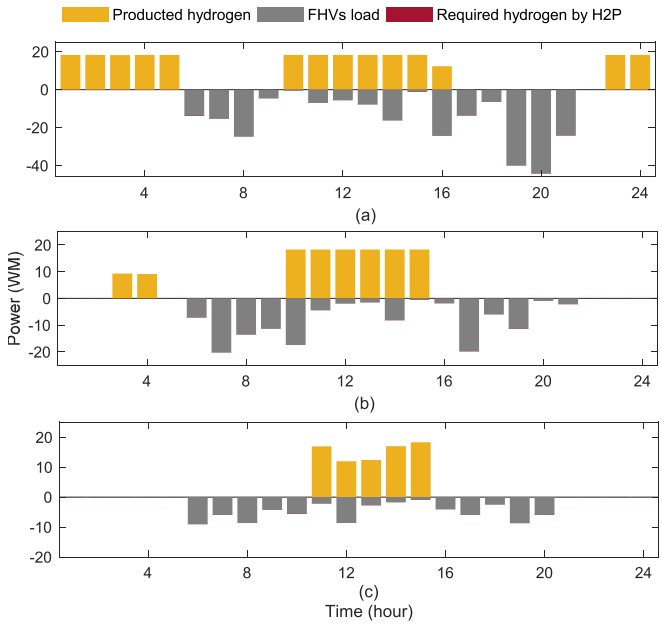

Fig. 7. The day-ahead hydrogen scheduling for (a) EHI-CS1; (b) EHI-CS2; and (c) EHI-CS3.

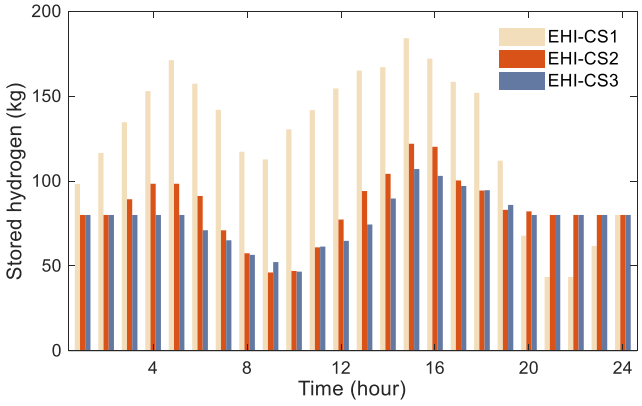

Fig. 8. The day-ahead stored hydrogen in different time intervals for three EHI-CSs.

4.3. *Real-time dispatch results*

Following the day-ahead scheduling results, the proposed MPC-based real-time optimization approach is developed to implement the real-time energy dispatch. The real-time dispatch performance for electric exchanged power with the gird over the test day is presented in Fig. 9.

The performance results of the real-time electricity, hydrogen dispatch and stored hydrogen are shown in Fig. 10, Fig. 11 and Fig. 12, respectively. The results are slightly different from the day-ahead scheduling results in Figs. 6, Figs. 7 and 8. It indicates that the real-time dispatch model can adjust the operational plans based on the up-to-date variables (e.g., PV power generation, PEV and HFV demands). It should be noted that the curtailment of PV occurs due to the forecasting errors and the additional penalty for the power imbalance in the RTM, as shown in Fig. 10. As the unplanned electricity sold to the grid will be penalized under this condition, the curtailment of PV power generation occurs.

Further, to validate the economic performance of the proposed

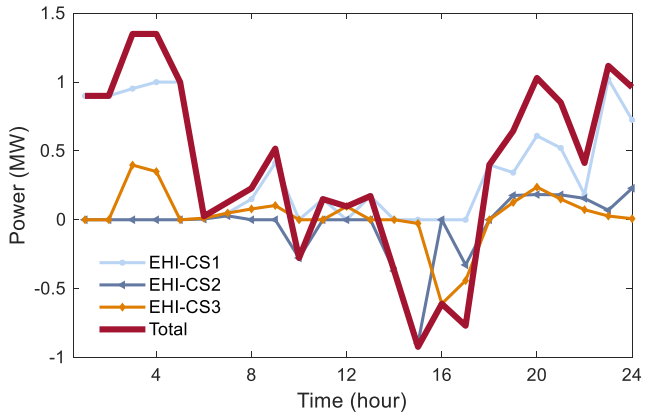

Fig. 9. The electric power exchange with the gird in the RTM dispatch stage.

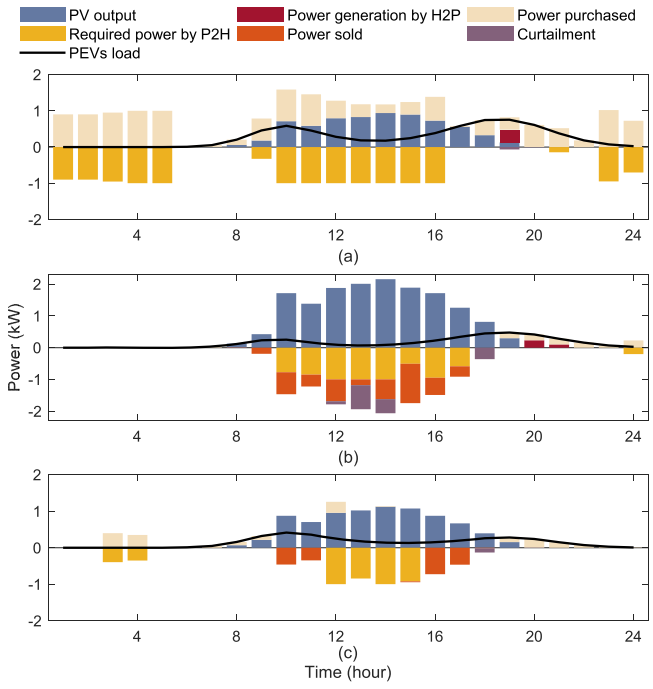

Fig. 10. Real-time electricity dispatch results for (a) EHI-CS1; (b) EHI-CS2; and (c) EHI-CS3.

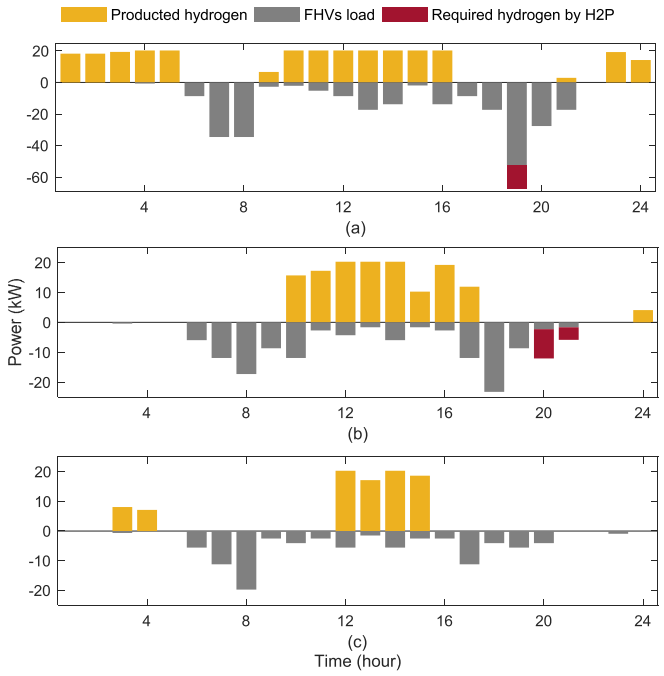

Fig. 11. Real-time hydrogen dispatch results for(a) EHI-CS1; (b) EHI-CS2; and (c) EHI-CS3.

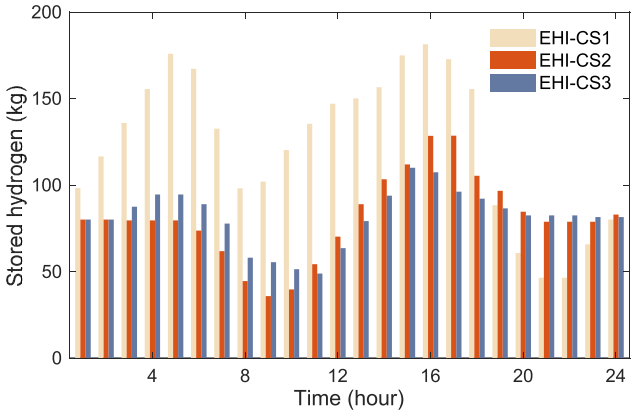

Fig. 12. Real-time stored hydrogen in different time intervals for three EHI-CSs.

energy management method over a period, the proposed solution is assessed over the period of 7 days in comparison with two benchmark solutions:

Benchmark 1: no electricity energy transaction between EHI-CSs.

Benchmark 2: the day-ahead scheduling plan is executed without any intra-day corrections.

Fig. 13 shows the day-ahead and actual net-load profiles for the whole multiple EHI-CSs unit compared with the benchmark 2 over 7 test days with the day-ahead clearing prices, PV power generation, PEV and HFV demands extracted from Refs. [15,37–41]. It can be observed that by applying MPC to online update the EHI-CSs control decisions, the actual unit net-load can generally follow the day-ahead scheduling plan with minor deviations. In contrast, the significantly larger deviations between the day-ahead and actual net-load deviations have occurred without control action update for the unit. Furthermore, based on Eq. (12) and Eq. (13), the actual operation cost over test days for the multiple EHI-CSs unit compared with two benchmark solutions are illustrated in Fig. 14. It is found that the proposed solution outperforms the other two benchmark solutions. In detail, the actual operational cost with the mean cost over 7 test days using the proposed solution is 712.2 $ which is a reduction of 9.59% compared with Benchmark1 (787.7 $). It can be also found that, on certain days, although the penalty cost in RTM of the proposed solution is greater than the benchmark1, the additional cost is smaller. This indicates that in addition to controllable facilities (i.e., HES systems), the multiple EHI-CSs unit includes an adjustment method in the proposed solution, i.e., energy transaction between EHI-CSs, allowing flexible coordination of day-ahead planning and real-time dispatching to reduce the actual daily operation cost. Besides, the average cost of using the proposed solution is 46.18% lower than Benchmark2 (1323.2 $). This suggests that the proposed method can effectively reduce the impact of prediction errors in the day-ahead scheduling through real-time dispatching.

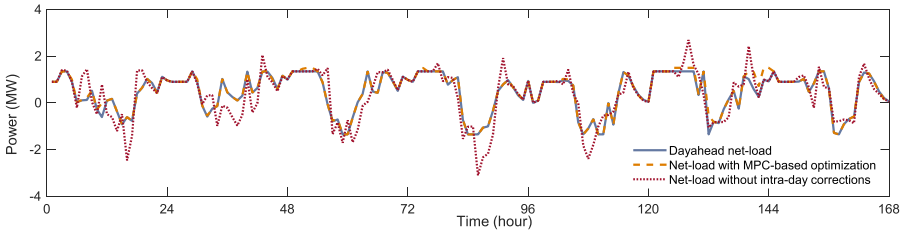

Fig. 13. Net-load profiles of day-ahead scheduling and real-time dispatch results with and without intra-day corrections (over 7 test days).

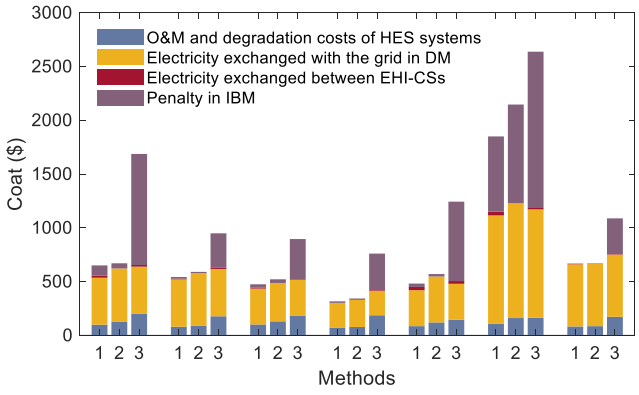

Fig. 14. Comparison of the operational cost over 7 test days. Note, 1: proposed solution; 2: benchmark 1; 3: benchmark 2.

4.4. Further analysis with consideration of V2G

It can be observed from Fig. 10 that the curtailment of PV power generation occurs due to the penalty mechanism in the RTM. The curtailment power of PV generation over 7 test days is illustrated in Fig. 15, and the mean curtailment power is 2.91 MW. To mitigate the PV power curtailment, the Vehicle-to-Grid (V2G) operation is considered. The V2G operation allows the PEV battery to absorb excess PV generation or low-cost electricity, which can be discharged when necessary to accommodate uncertainty or satisfy peak loads [47]. Although the fast-charging stations usually serve PEVs that need to be recharged immediately (typical charging duration of 30 min or less) [48], it cannot be ruled out that some PEVs can stay at EHI-CSs for a long time, e.g. owners who work nearby and are willing to provide V2G service. The studies in Refs. [49–51] confirmed the feasibility of integrating fast-charging V2G into the energy distribution. For the sake of simplicity, the following assumptions are made in this analysis: (1) 10 charging piles (about 0.4 MW capacity) are added to each EHI-CS can provide V2G services; (2) the initial SOC of each PEV battery providing V2G is set as 60% [49]; and (3) all the charging piles are occupied for V2G.

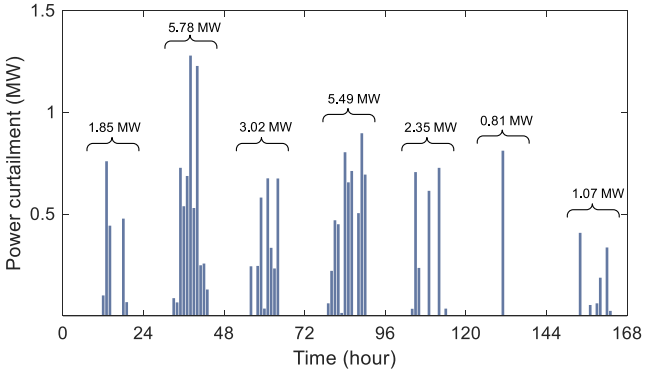

Fig. 15. Curtailment power of PV generation without V2G operation over 7 test days.

Here, the cost of V2G service provision is defined in Eq. (29) that needs to be considered in the objective function, as suggested in Ref. [52]. It is worth noting that V2G subsidy price is related to many factors, e.g. electricity market price and grid subsidy to V2G users. In practice, a trade-off needs to be made between setting the subsidy price and revenue of the EHI-CS [53]. In this work, the V2G subsidy from EHI-CSs is set as 0.02$/kWh.

$$F_t^{\mathrm{V2G}} = \sum_{m=1}^{M}\sum_{r=1}^{R} r_t^{\mathrm{PEV}} P_{m,r,t}^{\mathrm{PEV,disc}} \Big/ \eta^{\mathrm{PEV,disc}} \tag{29}$$

The charging and discharging process of PEVs is formulated in Eqs. (30)–(36). The SOC in the PEV battery is given by Eqs. (30) and (31). Eq. (32) ensures the charging and discharging processes will not occur at the same time, and Eqs. (33) and (34) limit the charging and discharging power. Ideally, the nominal capacity of a PEV's battery is 40 kWh with charging and discharging power of 40 kW (400 V/100 A) and 20 kW (400 V/50 A) [50], respectively, and charging and discharging efficiency of 95%, [51]. Eq. (35) limits the stored energy for every PEV battery within 20–95%, and Eq. (36) signifies the charging requirement of each PEV should be satisfied upon its departure time. The power balance for individual EHI-CSs is given in Eq. (37).

$$SOC_{m,r,t}^{\mathrm{PEV}} = SOC_{m,r,t-1}^{\mathrm{PEV}} + \frac{P_{m,r,t}^{\mathrm{PEV,ch}}\eta^{\mathrm{PEV,ch}} - P_{m,r,t}^{\mathrm{PEV,disc}} \Big/ \eta^{\mathrm{PEV,disc}}}{C_{m,r,t}^{\mathrm{PEV}}}, t \in \left(\Gamma_{m,r}^{\mathrm{arr}}, \Gamma_{m,r}^{\mathrm{dep}}\right] \tag{30}$$

$$SOC_{m,r,t}^{\mathrm{PEV}} = SOC_{m,r}^{\mathrm{PEV,ini}} + \frac{P_{m,r,t}^{\mathrm{PEV,ch}}\eta^{\mathrm{PEV,ch}} - P_{m,r,t}^{\mathrm{PEV,disc}} \Big/ \eta^{\mathrm{PEV,disc}}}{C_{m,r,t}^{\mathrm{PEV}}}, t = \Gamma_{m,r}^{\mathrm{arr}} \tag{31}$$

$$I_{m,r,t}^{\mathrm{PEV,disc}} + I_{m,r,t}^{\mathrm{PEV,ch}} \le 1 \tag{32}$$

$$0 \le P_{m,r,t}^{\mathrm{PEV,disc}} \le DR_{\max}^{\mathrm{PEV}} I_{m,r,t}^{\mathrm{PEV,disc}} \tag{33}$$

$$0 \le P_{m,r,t}^{\mathrm{PEV,ch}} \le CR_{\max}^{\mathrm{PEV}} I_{m,r,t}^{\mathrm{PEV,ch}} \tag{34}$$

$$SOC_{\min}^{\mathrm{PEV}} \le SOC_{m,r,t}^{\mathrm{PEV}} \le SOC_{\max}^{\mathrm{PEV}} \tag{35}$$

$$SOC_{m,r,t}^{\mathrm{PEV}} \le SOC_{m,r}^{\mathrm{PEV,dep}} \tag{36}$$

$$P_{\mathrm{used},m,t}^{\mathrm{Solar}} + P_{m,t}^{\mathrm{H2P}} - P_{m,t}^{\mathrm{P2H}} - P_{m,t}^{\mathrm{PEV}} - \sum_r P_{m,r,t}^{\mathrm{EV,ch}} + \sum_r P_{m,r,t}^{\mathrm{PEV,disc}} = P_{\mathrm{all},m,t}^{\mathrm{sell}} - P_{\mathrm{all},m,t}^{\mathrm{buy}} \tag{37}$$

With the V2G operation, the curtailment power of PV generation over 7 test days are shown in Fig. 16. The result indicates that the V2G operation can efficiently mitigate the PV power curtailment with the mean curtailment power of 2.28 MWh, i.e. a 21.65% reduction compared with the scenario without V2G.

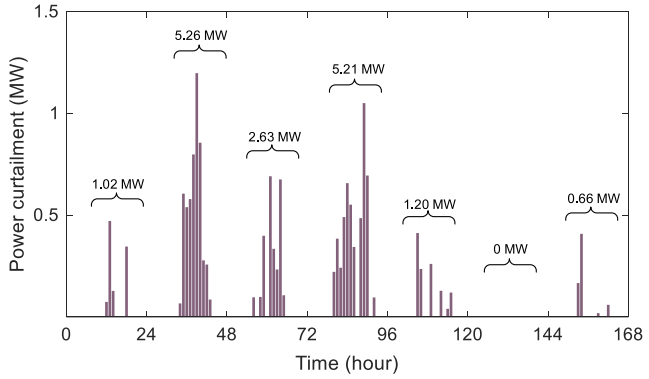

Fig. 16. Curtailment power of PV generation with V2G operation over 7 test days.

5. Conclusions and future work

In this paper, a two-stage EMS strategy is presented for multiple EHI-CSs unit to meet the electric and hydrogen demands of vehicles simultaneously. A set of interconnected EHI-CSs in the designed system can realize the power coordination among multiple EHI-CSs, and the HES system consisting of the P2H, H2P and hydrogen storage tanks is utilized to accommodate the intermittency of PV power generation in the electricity market. The flexible coordination of day-ahead scheduling and real-time dispatch is implemented in the deregulated power market. In the day-ahead scheduling stage, the EHI-CSs aggregator aims to minimize the cost of the whole multiple EHI-CSs unit based on the day-ahead clearing price and the day-ahead forecasted data through economic optimization. In the real-time dispatching stage, the MPC-based real-time dynamic dispatch is carried out to minimize the penalty cost based on the day-ahead scheduling and short-term forecasted data. The proposed two-stage EMS strategy for the multiple EHI-CSs unit is assessed through extensive simulation experiments compared with two benchmark solutions. The numerical results indicate that the proposed solution outperforms the two benchmark solutions with mean daily actual operational costs reduced by 9.59% and 46.18%, respectively. In addition, further analysis is provided to assess the benefits of V2G operation and the numerical results show that a 21.65% reduction of PV power curtailment in the condition that 0.4 MW of V2G capacity is added to each EHI-CS.

For future work, a number of research directions are considered worth further effort. The proposed solution needs to be further exploited and validated in the off-grid operation with multiple EHI-CSs system through experiments. Also, the cost-benefit analysis of V2G operation in the energy management is required to further elaborated and quantified for different V2G capacities.

Credit author statement

Xiaolun Fang: Conceptualization, Methodology, Data curation, Writing, Original draft preparation. Yubin Wang: Visualization. Wei Dong: Investigation. Yang Qiang: Supervision, Reviewing and Editing, Siyang Sun: Provide PEVs data.

Declaration of competing interest

The authors declare that they have no known competing financial interests or personal relationships that could have appeared to influence the work reported in this paper.

Data availability

Data will be made available on request.

Acknowledgments

This work is supported by the Natural Science Foundation of China (52177119) and the Technology Research and Development Program of Zhejiang Province (2022C01239).

References

[1] Wahedi AA, Bicer Y. Development of an off-grid electrical vehicle charging station hybridized with renewables including battery cooling system and multiple energy storage units. Energy Rep 2020;6:2006–21.
[2] Wang L, Jiao S, Xie Y, et al. Two-way dynamic pricing mechanism of hydrogen filling stations in electric-hydrogen coupling system enhanced by blockchain. Energy 2022;239.
[3] Xiao W, Cheng Y, Lee WJ, Chen V, Charoensri S. Hydrogen filling station design for fuel cell vehicles. IEEE Trans Ind Appl 2011;47(1):245–51.
[4] Bertuccioli L, Chan A, Hart D, et al. Development of water electrolysis in the European union. Episodes 2014;31(1):140–7. 2014.
[5] Daneshvar M, Ivatloo BM, Zare K, Asadi S. Transactive energy management for optimal scheduling of interconnected microgrids with hydrogen energy storage. Int J Hydrogen Energy 2021;46(30):16267–78.
[6] Zhang H, Chen Y, Liu K, Dehan S. A novel power system scheduling based on hydrogen-based micro energy hub. Energy 2022;251.
[7] Apostolou D, Xydis G. A literature review on hydrogen refuelling stations and infrastructure Current status and future prospects. Renew Sustain Energy Rev 2019;113.
[8] Wu X, Qi S, Wang Z, Duan C, Wang X, Li F. Optimal scheduling for microgrids with hydrogen fueling stations considering uncertainty using data-driven approach. Appl Energy 2019;253.
[9] Mehrjerdi H. Off-grid solar powered charging station for electric and hydrogen vehicles including fuel cell and hydrogen storage. Int J Hydrogen Energy 2019;44(23):11574–83.
[10] Kuvvetli Y. Multi-objective and multi-period hydrogen refueling station location problem. Int J Hydrogen Energy 2020;45(55).
[11] Thiel D. A pricing-based location model for deploying a hydrogen fueling station network. Int J Hydrogen Energy 2020;45(46):24174–89.
[12] Panah PG, Bornapour M, Hemmati R, Guerrero JM. Charging station stochastic programming for hydrogen/battery electric buses using multi-criteria crow search algorithm. Renew Sustain Energy Rev 2021;144.
[13] El-Taweel NA, Khani H, Farag HEZ. Hydrogen storage optimal scheduling for fuel supply and capacity-based demand response program under dynamic hydrogen pricing. IEEE Trans Smart Grid 2019;10(4):4531–42.
[14] Wu X, Li H, Wang X, Zhao W. Cooperative operation for wind turbines and hydrogen fueling stations with on-site hydrogen production. IEEE Trans Sustain Energy 2020;11(4):2775–89.
[15] Khani H, El-Taweel NA, Farag HEZ. Supervisory scheduling of storage-based hydrogen fueling stations for transportation sector and distributed operating reserve in electricity markets. IEEE Trans Ind Inf 2020;16(3):1529–38.
[16] Saatloo AM, Ebadi R, Mirzaei MA, et al. Multi-objective IGDT-based scheduling of low-carbon multi-energy microgrids integrated with hydrogen refueling stations and electric vehicle parking lots. Sustain Cities Soc 2021;74.
[17] Mehrjerdi H, Hemmati R. Wind-hydrogen storage in distribution network expansion planning considering investment deferral and uncertainty. Sustain Energy Technol Assessments 2020;39.
[18] Mirzaei MA, Yazdankhah AS, Ivatloo BM. Stochastic security-constrained operation of wind and hydrogen energy storage systems integrated with price-based demand response. Int J Hydrogen Energy 2019;44(27):14217–27.
[19] Pan G, Gu W, Lu Y, Qiu H, Lu S, Yao S. Optimal planning for electricity-hydrogen integrated energy system considering power to hydrogen and heat and seasonal storage. IEEE Trans Sustain Energy 2020;11(4):2662–76.
[20] Teng Y, Wang Z, Li Y, Ma Q, Hui Q, Li S. Multi-energy storage system model based on electricity heat and hydrogen coordinated optimization for power grid flexibility. CSEE J Power Energy Syst 2019;5(2):266–74.
[21] Liu W, Zhuang P, Liang H, Peng J, Huang Z. Distributed economic dispatch in microgrids based on cooperative reinforcement learning. IEEE Transact Neural Networks Learn Syst June 2018;29(6):2192–203.
[22] Dai P, , W. Y u, Wen G, Baldi S. Distributed reinforcement learning algorithm for dynamic economic dispatch with unknown generation cost functions. IEEE Trans Ind Inf Apr. 2020;16(4):2258–67.
[23] Ganesh AH, Xu B. A review of reinforcement learning based energy management systems for electrified powertrains: progress, challenge, and potential solution. Renew Sustain Energy Rev 2022;154.
[24] Gu W, Wang Z, Wu Z, Luo Z, Tang Y, Wang J. An online optimal dispatch schedule for CCHP microgrids based on model predictive control. IEEE Trans Smart Grid 2017;8(5):2332–42.
[25] Batiyaha S, Sharma R, Abdelwahed S, Zohrabi N. An MPC-based power management of standalone DC microgrid with energy storage. Electric Power Energy Syst 2020;120.

[26] Lakouraj MM, Niaz H, Liu JJ, Siano P, Moghaddam AA. Optimal risk-constrained stochastic scheduling of microgrids with hydrogen vehicles in real-time and day-ahead markets. J Clean Prod 2021;318.
[27] Garcia-Torres F, Bordons C. Optimal economical schedule of hydrogen-based microgrids with hybrid storage using model predictive control. IEEE Trans Ind Electron 2015;62(8):5195–207.
[28] Dibavar AA, Tabar VS, Zadeh SG, Nourollahi R. Two-stage robust energy management of a hybrid charging station integrated with the photovoltaic system. Int J Hydrogen Energy 2021;46(24):12701–14.
[29] Khavari F, Badri A, Zangeneh A. Energy management in multi-microgrids considering point of common coupling constraint. Int J Electr Power Energy Syst 2020;115.
[30] Nikmehr N, Ravadanegh SN, Khodaei A. Probabilistic optimal scheduling of networked microgrids considering time-based demand response programs under uncertainty. Appl Energy 2017;198:267–79.
[31] Zheng Y, Yu H, Shao Z, Jian L. Day-ahead bidding strategy for electric vehicle aggregator enabling multiple agent modes in uncertain electricity markets. Appl Energy 2020;280:115977.
[32] Luo F, Ranzi G, Wan C, Xu Z, Dong ZY. A multistage home energy management system with residential photovoltaic penetration. IEEE Trans Ind Inf 2019;15(1):116–26.
[33] Das S, Basu M. Day-ahead optimal bidding strategy of microgrid with demand response program considering uncertainties and outages of renewable energy resources. Energy 2020;190:1–13.
[34] Yoldas Y, Goren S, t Onen A, Ustun TS. Dynamic rolling horizon control approach for a university campus. Energy Rep 2022;1:1154–62.
[35] Petrollese M, Valverde L, Cocco D, et al. Real-time integration of optimal generation scheduling with MPC for the energy management of a renewable hydrogen-based microgrid. Appl Energy 2016;166:96–106.
[36] IBM ILOG CPLEX. CPLEX optimizer. [Online]. Available: https://www.ibm.com/docs/en/icos/20.1.0?topic=mc-what-is-cplex.
[37] Schoenung S. Economic analysis of large-scale hydrogen storage for renewable utility applications. Sandia National Laboratories; 2011.
[38] Tostado-Veliz M, Kamel S, Hasanien HM, et al. A mixed-integer-linear-logical programming interval-based model for optimal scheduling of isolated microgrids with green hydrogen-based storage considering demand response. J Energy Storage 2022;48.
[39] ISO New England. Day-ahead hourly locational marginal price,accessed on Feb. 10, 2016. [Online]. Available: http://www.iso-ne.com/isoexpress/web/reports/pricing/-/tree/lmps-da-hourly.
[40] University of Queensland, Weather and local environment. Available: http://www.uq.edu.au/solarenergy/pv-array/weathe.
[41] Sun S, Yang Q, Yan W. Hierarchical optimal planning approach for plug-in electric vehicle fast charging stations based on temporal-SoC charging demand characterisation. IET Gener, Transm Distrib 2018;12:4388–95.
[42] Dong W, Yang Q, Fang X, Ruan W. Adaptive optimal fuzzy logic based energy management in multi-energy microgrid considering operational uncertainties. Appl Soft Comput J 2021;98. 106882.
[43] Dong W, Yang Q, Li W, Zomaya AY. Machine learning based real-time economic dispatch in islanding microgrids in a cloud-edge computing environment. IEEE Internet Things J 2021;8(17):13703–11.
[44] Ge X, Shi L, Fu Y, et al. Data-driven spatial-temporal prediction of electric vehicle load profile considering charging behavior. Elec Power Syst Res 2020;187:106469.
[45] Yu L, Jiang T, Cao Y. Energy cost minimization for distributed internet data centers in smart microgrids considering power outages. IEEE Trans Parallel Distr Syst 2015;26(1):120–30.
[46] Wang Y, Dong W, Yang Q. Multi-stage optimal energy management of multi-energy microgrid in deregulated electricity markets. Appl Energy 2022;310.
[47] Elliott M, Kittner N. Operational grid and environmental impacts for a V2G-enabled electric school bus fleet using DC fast chargers. Sustain Prod Consum 2022;30:316–30.
[48] Yang Q, Sun S, Deng S, Zhao Q, Zhou M. Optimal sizing of PEV fast charging stations with markovian demand characterization. IEEE Trans Smart Grid 2019;10(4):4457–66.
[49] Das HS, Li S, Chowdhury MFF, Ghosh T. Game theoretical energy management of EV fast charging station with V2G capability. IEEE International Conference on Power and Energy (PECon); 2020. p. 344–9. 2020.
[50] George MA, Rao GK, Jena P. Performance analysis of fast charging stations for G2V and V2G microgrid systems. 2020 21st National Power Systems Conference (NPSC); 2020. p. 1–6.
[51] Mazumder M, Debbarma S. EV charging stations with a provision of V2G and voltage support in a distribution network. IEEE Syst J 2021;15(1):662–71.
[52] Gao S, Chau KT, Liu C, Wu D, Chan CC. Integrated energy management of plug-in electric vehicles in power grid with renewables. IEEE Trans Veh Technol 2014;63(7):3019–27.
[53] Pelletier S, Jabali O, Laporte G, et al. Battery degradation and behavior for electric vehicles: review and numerical analyses of several models. Transport Res Part B 2017;103:158–87.